



Assessment of damages in fault rupture–shallow foundation interaction due to the existence of underground structures

Alireza Saeedi Azizkandi^{a,*}, Sadegh Ghavami^a, Mohammad Hasan Baziar^a,
Sajjad Heidari Hasanaklou^b

^a School of Civil Engineering, Iran University of Science and Technology, Tehran, Iran

^b Center of Excellence for Fundamental Studies in Structural Engineering, School of Civil Engineering, Iran University of Science and Technology, Tehran, Iran

ARTICLE INFO

Keywords:

Fault rupture
Tunnel
Shallow foundation
Numerical simulation

ABSTRACT

Permanent ground deformations induced by fault movements can be damaging to engineering structures built on or near active faults. Most experimental and numerical studies have so far confirmed the fact that the presence of a tunnel in the vicinity of an active fault can change the zone of large deformations on the ground surface. This paper investigates the effect of tunnel existence on the interaction between a reverse fault and a shallow foundation using the finite element method. This paper also analyzes the manner in which a foundation in faulting zones responds to various parameters such as foundation position, tunnel depth and diameter, and the position of the tunnel relative to the rupture path in free-field condition. The mechanical response of the tunnel lining is also examined. The results show that the existence of a tunnel, in some cases, can increase the foundation rotation. Varying the tunnel diameter did not cause any significant changes in the general pattern of failure and the location of shear planes near the tunnel. However, a tunnel with a larger diameter causes the rupture to deviate and propagate in a wider area of the soil layer. It was found that increasing the tunnel depth extends a branch of the rupture path towards the footwall and expands the shear zone on a wider area. In the end, this paper examines the effectiveness of expanded polystyrene sheet (EPS) walls in mitigating the surface fault rupture and reducing the foundation rotation.

1. Introduction

Earthquake movements and displacements can be classified into two main categories: (a) ground shakings triggered by seismic waves and (b) permanent ground deformations induced by fault movements (Karamanos et al., 2017). If the fault movement propagates up to or near the ground surface, faulting can cause significant damage to a structure, especially when it is accompanied by strong ground shakings (Lazarte, 1996). The 1999 Kocaeli and Düzce-Bolu earthquakes in Turkey (Lettis et al., 2000; Ulusay et al., 2002; Pamuk et al., 2005) and the 1999 Chi-Chi earthquake in Taiwan (Tsai et al., 2000; Schiff and Tang, 2000; Lew et al., 2000; Kelson et al., 2001) are among numerous examples illustrating the severe damages caused by permanent ground deformations to buildings and infrastructures. It should be noted that this research does not cover the subject of wave transition induced by earthquakes.

Research on the subject of fault rupture propagation through soil can be generally classified into four categories:

- real case histories (Bray, 2001; Konagai, 2005; Anastasopoulos and Gazetas, 2007a; Faccioli et al., 2008)
- experimental methods based on physical modeling (El Nahas et al., 2006; Lin et al., 2007; Bransby et al., 2008a,b; Anastasopoulos et al., 2009; Ahmed and Bransby, 2009; Moosavi et al., 2010; Loli et al., 2012; Baziar et al., 2014b; Ashtiani et al., 2016)
- numerical analyses (Gazetas et al., 2007; Anastasopoulos and Gazetas, 2007b; Anastasopoulos et al., 2008a; Oettle and Bray, 2013a; Baziar et al., 2014a)
- analytical studies (Berrill, 1983; Yilmaz and Paolucci, 2007; Anastasopoulos et al., 2008b,c).

1.1. Interaction of fault with shallow foundation

The interaction of dip-slip faults with shallow foundations has been investigated by several researchers using experimental modeling (El Nahas et al., 2006; Bransby et al., 2008a,b; Anastasopoulos et al., 2009; Ahmed and Bransby, 2009; Moosavi et al., 2010; Ashtiani et al., 2016) and numerical analyses (Gazetas et al., 2007; Anastasopoulos and

* Corresponding author.

E-mail addresses: asaedia@iust.ac.ir (A.S. Azizkandi), s_ghavamijamal@civileng.iust.ac.ir (S. Ghavami), baziar@iust.ac.ir (M.H. Baziar).

Nomenclature			
B	foundation width	d_{FE}	finite-element size
c	cohesion	γ_f^p	octahedral plastic shear strain at the end of softening
D	tunnel diameter	γ_{oct}^p	octahedral plastic shear strain
D_r	relative density	θ_1	foundation rotation without a tunnel
h	vertical throw of hanging wall	θ_2	foundation rotation in the presence of the tunnel
H	depth of EPS wall	θ_3	foundation rotation in the presence of the tunnel and EPS wall
R	tunnel radius	μ	coefficient of friction
S	Horizontal distance between foundation left corner and point of rupture emergence in the free field	φ	friction angle of soil
t	thickness of tunnel lining	φ_{mob}	mobilized friction angle of soil
w	width of EPS wall	φ_p	friction angle of soil at peak
x	horizontal distance between the tunnel center and fault rupture in the free field	φ_{res}	residual friction angle of soil
y	vertical distance between the tunnel center and the ground surface	ψ	dilation angle of soil
		ψ_{mob}	mobilized dilation angle of soil
		ψ_p	dilation angle of soil at peak
		ψ_{res}	residual dilation angle of soil

Gazetas, 2007b; Anastasopoulos et al., 2008a; Baziar et al., 2014a). The foundation could deviate the fault rupture away from itself, leaving it almost undisturbed (Bray, 2001; Bransby et al., 2008b). The rigidity and continuity of the foundation and increasing structural weight improve the performance of foundation (Anastasopoulos and Gazetas, 2007b; Anastasopoulos et al., 2008a; Baziar et al., 2014a). In addition, the interaction between the shallow foundations and fault ruptures is very sensitive to the position of the foundation relative to the fault outcrop location (Bransby et al., 2008a,b; Baziar et al., 2014a). Embedding the foundation changes the mechanism of the fault rupture–foundation interaction, thereby, causing a significant rotation and an unfavorable performance (Ashtiani et al., 2016). A building would fail by either the fault rupture or excess rotation of its foundation (Brennan et al., 2007).

A continuous and rigid foundation could perform as a cantilever or a simply supported beam, bridging the locally generated gaps and drastically reducing the distress of the superstructure. Nevertheless, even a rigid body rotation may condemn the operation of a facility (Fadaee et al., 2013), and, therefore, special attention must be given to the

rotation of foundation.

Although the prevailing strategy for mitigating the surface fault rupture hazard is to avoid building on or near active fault traces, it is not always a viable option (Oettle, 2013). A number of hazard mitigation techniques have been proposed in technical literature. Moosavi and Jafari (2012) investigated the application of geosynthetic layers in the soil beneath the structure through physical and numerical modeling. Fadaee et al. (2013) used a soil bentonite wall, placed between the outcropping dislocation and the foundation, to protect foundation–structure systems from a thrust fault. Oettle and Bray (2013b) studied the effectiveness of geotechnical mitigation strategies such as ground improvement by densification of the soil beneath a structure, installing a diaphragm wall between the bedrock fault and the structure, and tying a structure down with stiff ground anchors. Ashtiani et al. (2018) carried out a series of centrifuge tests to evaluate the effectiveness of two mitigation measures to decrease the hazards associated with reverse faulting on shallow embedded foundations. These measures included the vertical trench adjacent to the foundation and a reinforced zone with high density polyethylene geogrid beneath the

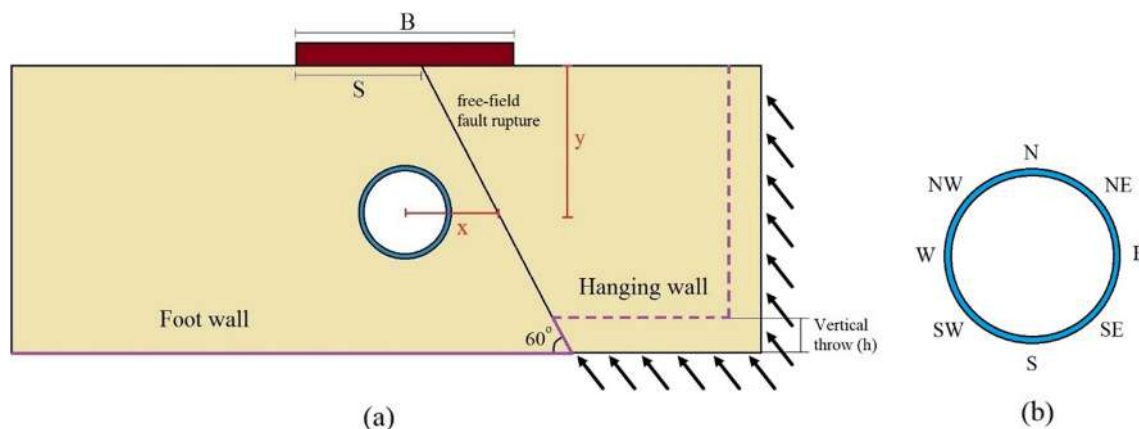


Fig. 1. (a) A schematic view of the numerical model; (b) principal and intermediate directions of the tunnel cross section.

Table 1

List of numerical modeling with the parameters considered in the analysis.

Parameters	S/B, B = 8.5 m	x	y	D
Effect of the presence of tunnel on reverse fault–foundation interaction	0–1	–3R to 3R	8 m	4 m
The effect of tunnel diameter on the reverse fault–foundation interaction	0–0.75	–3R to 3R	8 m	4 m and 6 m
The effect of tunnel depth on reverse fault–foundation interaction	0–0.75	–3R to 3R	8 m and 10 m	4 m

Table 2
The properties of the material adopted in the numerical simulation.

Material properties	Value
Tunnel:	
Unit weight (kN/m ³)	24
Elastic modulus (GPa)	25
Poisson's ratio	0.28
Foundation:	
Unit weight (kN/m ³)	78.6
Elastic modulus (GPa)	200
Poisson's ratio	0.35
Soil:	
Unit weight (kN/m ³)	15.65
Elastic modulus (MPa)	20
Poisson's ratio	0.3
Cohesion, c (kPa)	0.5
φ_p (deg)	35
ψ_p (deg)	6
φ_{res} (deg)	30.2
Soil-Tunnel:	
Friction coefficient, μ	0.4
Soil-Foundation:	
Friction coefficient, $0.7\tan(\varphi)$	0.5

foundation. The trenches were filled with one of the following materials: (1) lightweight expanded clay aggregate, (2) a clay mixture composed of kaolinite and water, and (3) expanded polystyrene sheets

Table 3
Mechanical properties of the EPS used in numerical modeling.

Unit weight (kN/m ³)	Elastic modulus (kPa)	Poissons' ratio	Friction coefficient
0.117	3300	0.07	0.6

(EPS). The results showed that EPS-filled trenches completely absorbed the plastic shearing deformation and diverted the reverse fault rupture away from the foundation.

1.2. Interaction between fault and tunnel

The 21st century continues to see a rapidly growing demand for underground space use in city areas. Underground tunnels in densely populated Iranian cities such as Tehran are often constructed across fault zones, as it is not always possible to avoid crossing active faults. In such circumstances, earthquake-induced fault movements may subject the tunnel to differential displacements and generate stress concentrations (Wang et al., 2012). The fault movement may affect not only adjacent surfaces and underground structures, but also the tunnel itself (Sarayloo and Mahinroosta, 2016). As different types of tunnels experienced severe damages during earthquake fault ruptures (Ulusay et al., 2002; Prentice and Ponti, 1997; Wang et al., 2001; Sugimura et al., 2001; Konagai et al., 2005), a lot of research has been carried out through various methods on the response of tunnels located in the fault zone. Experimental and numerical results confirmed that the presence of a tunnel, depending on the tunnel position, depth, rigidity and soil

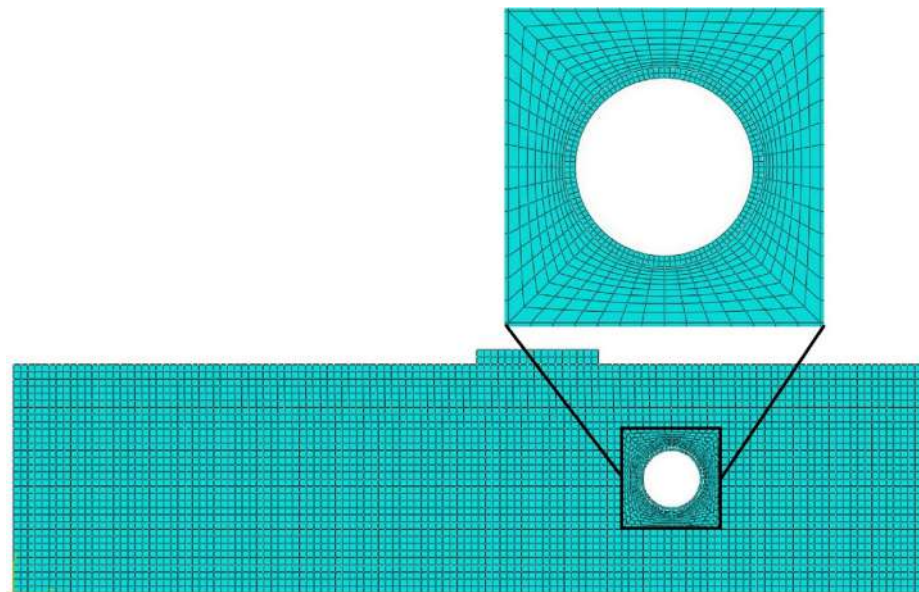


Fig. 2. Finite-element meshes used in the numerical analysis.

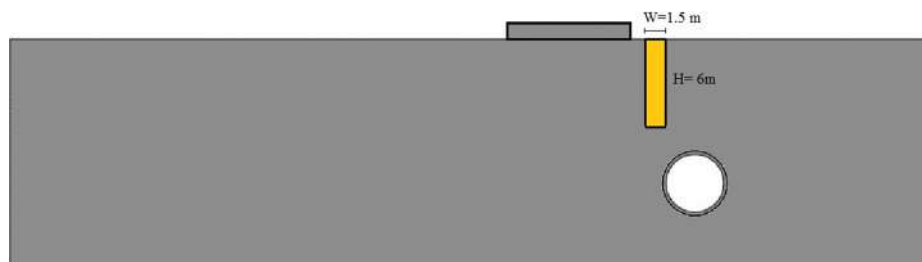


Fig. 3. A schematic view of the trench filled with EPS near the foundation.

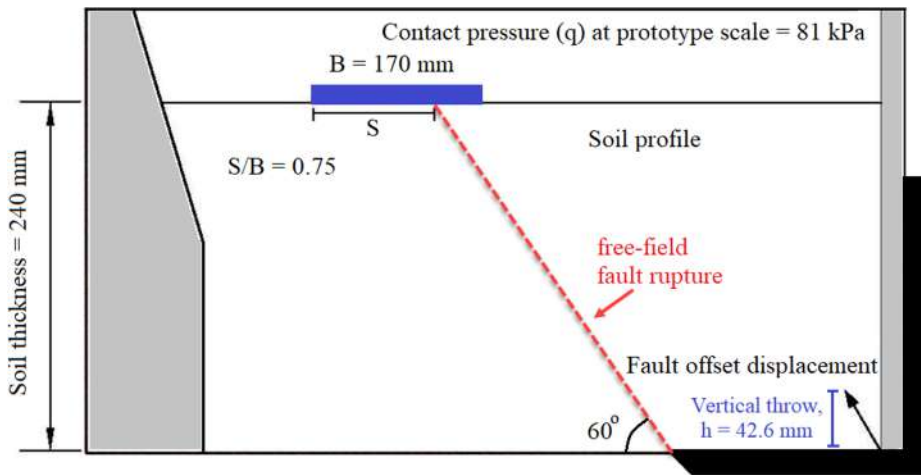


Fig. 4. Schematic configuration of the shallow foundation–fault rupture model (after Ashtiani et al., 2016).

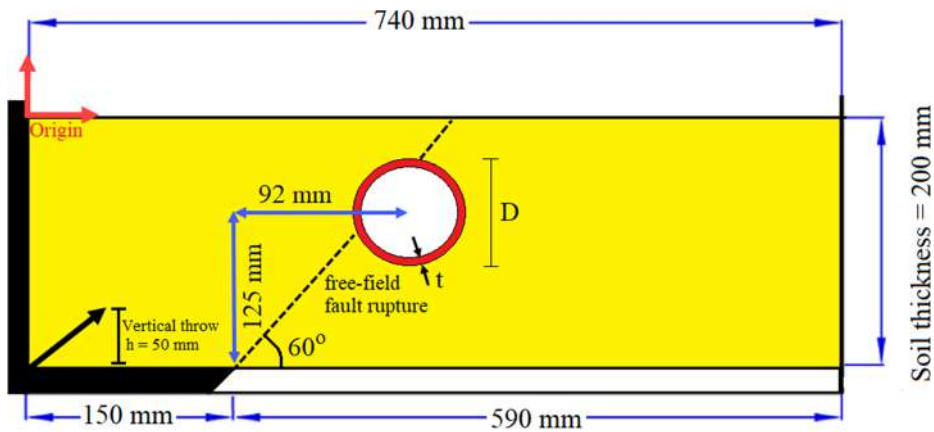


Fig. 5. Schematic configuration of the test (after Baziar et al., 2014b).

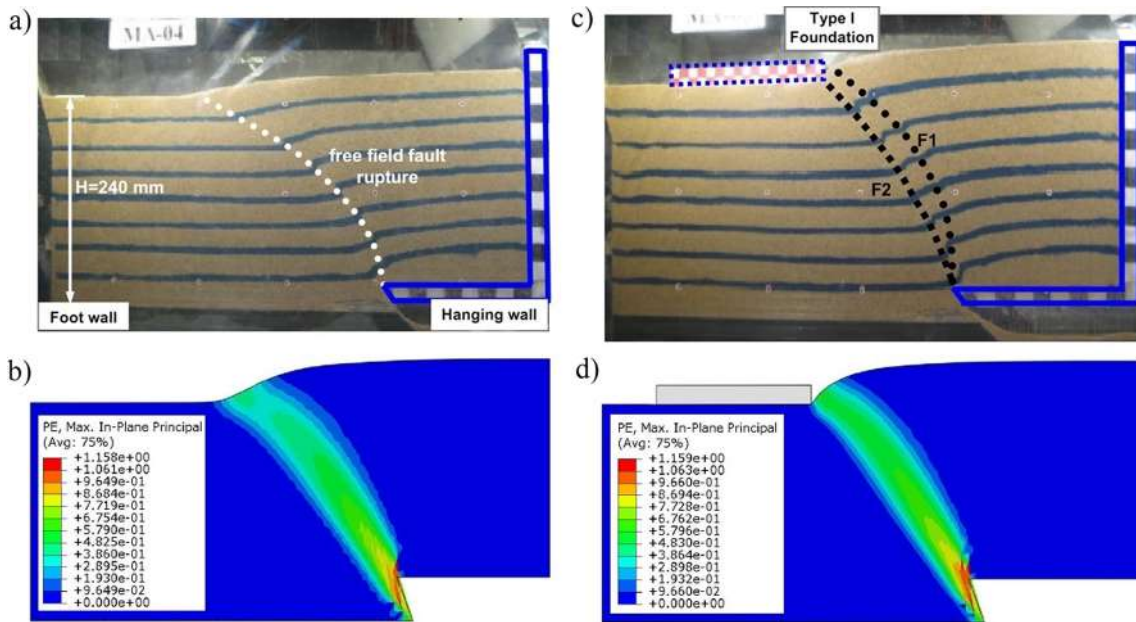


Fig. 6. Comparison between the numerical analysis and centrifuge results: (a) centrifuge model for the free-field, (b) deformed mesh with plain strain contours for the free-field condition in finite element analysis, (c) centrifuge model for the test with foundation was positioned at $S/B = 0.75$, (d) deformed mesh with plain strain contours for the test with foundation was positioned at $S/B = 0.75$ in finite element analysis.

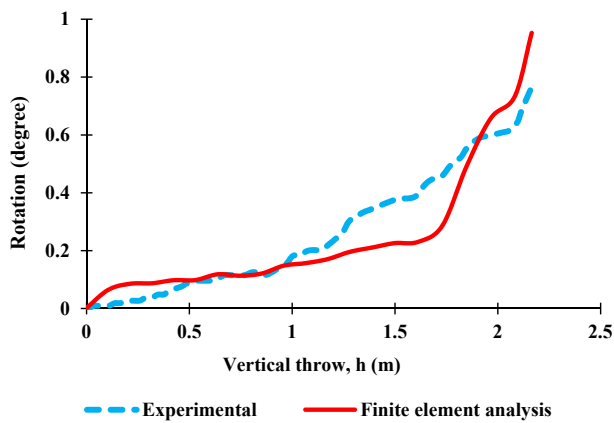


Fig. 7. Foundation rotation versus vertical throw of the fault.

relative density, deviates fault rupture and influences the large deformation zone on the ground surface due to faulting (Baziar et al., 2016). Tunnel location is one of the most crucial factors affecting the fault rupture path (Lin et al., 2007; Anastasopoulos and Gazetas, 2010; Sarayloo and Mahinroosta, 2016; Baziar et al., 2016). Depending on the position of the tunnel against the fault plane, the existing tunnel may either increase or decrease the surface settlement along the tunnel (Sarayloo and Mahinroosta, 2016). The investigation of the effects of faulting on shallow segmental tunnels using physical modeling showed that the formation of a sinkhole is primarily caused by the separation of tunnel segments. This ascertains that faulting not only damages a tunnel, but also threatens the adjacent surface structures (Kiani et al., 2016).

As mentioned, the existence and location of an underground tunnel can affect both the shear zone and ground surface displacement. The simultaneous effect of a foundation and tunnel on a surface fault rupture has not yet been investigated. In this research, the impact of the tunnel on the interaction between reverse fault and shallow foundation is numerically investigated. The effects of foundation position, tunnel

depth and the horizontal tunnel distance relative to the rupture path in free-field condition as well as the tunnel diameter on the foundation response in fault zone are investigated in this research. Furthermore, the effectiveness of a trench filled with EPS near the foundation on fault rupture-foundation-tunnel interaction for cases where the tunnel causes significant foundation rotation is also investigated in this research. Previous studies have revealed the numerical modeling based on the finite element method to be successful in studying the effect of fault on surface and underground structures (Lin et al., 2007; Gazetas et al., 2007; Anastasopoulos et al., 2008a; Anastasopoulos and Gazetas, 2010; Baziar et al., 2014a; Baziar et al., 2016). The FE software ABAQUS (2014) was used to conduct the numerical study. The numerical model has to be adequately validated with real case histories or experimental data. The numerical analysis of this research was verified with the findings of Ashtiani et al. (2016) on the reverse fault-foundation interaction modeled in centrifuge testing and Baziar et al. (2014b) on centrifuge modeling of interaction between reverse faulting and tunnel.

2. Numerical modeling method

The numerical analysis was conducted under two-dimensional plane strain condition by the ABAQUS software, based on the finite element approach.

Fig. 1 shows the configuration of the numerical model used in this study. The length and the depth of the soil profile were 64 m and 16 m, respectively, and the length was four times the depth (Gazetas et al., 2008). The foundation width (B) and thickness were 8.5 m and 1 m, respectively, and placed in different positions (S/B). Parameter S indicates the distance between the left corner of the foundation and the fault outcrop on the surface in free-field condition. A tunnel with diameter of D and thickness of $t = 0.24$ m was placed at different coordinates relative to free-field fault rupture path, as shown in Fig. 1(a). The distance between the tunnel center and the ground surface is indicated by “y”. If the tunnel is located in the hanging wall (the displaced side of the fault), “x” is positive, and if it is located in the footwall (the fixed side of the fault), “x” is negative. List of numerical modeling along with the parameters considered in the analysis is shown

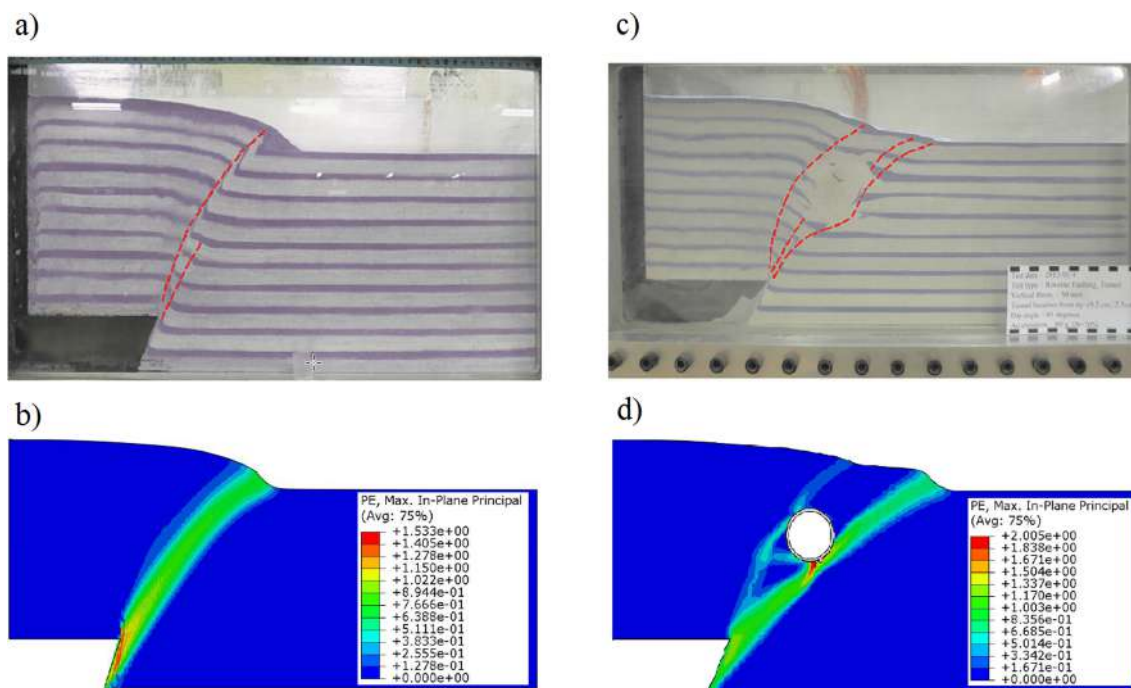


Fig. 8. Comparison between the numerical analysis and centrifuge results: (a) centrifuge model for the free-field, (b) deformed mesh with plain strain contours for the free-field condition in finite element analysis., (c) centrifuge model for the test with tunnel, (d) deformed mesh with plain strain contours for the test with tunnel in finite element analysis.

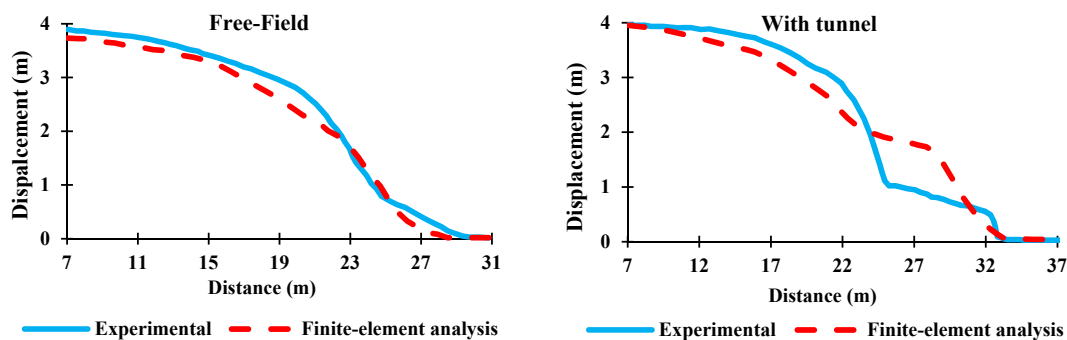


Fig. 9. Vertical displacement of the surface when fault throw is 4 m.

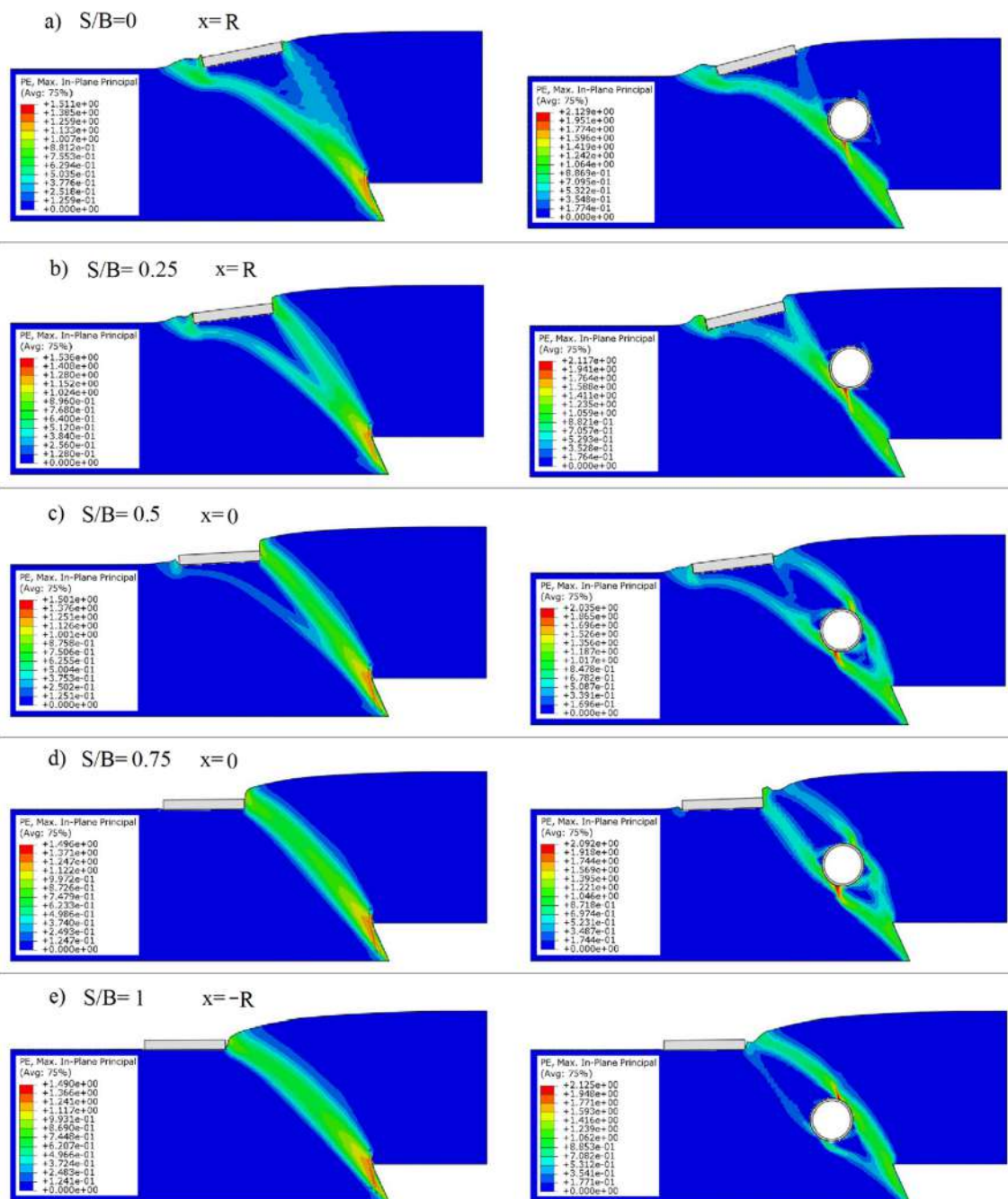


Fig. 10. The effect of the presence of a tunnel, $D = 4$ m in diameter, embedded in depth of $y = 8$ m, on reverse fault (60°)–foundation interaction (FE computed plastic strain contours) at $h = 4$ m. x is horizontal distances from the rupture path. R is the tunnel radius.

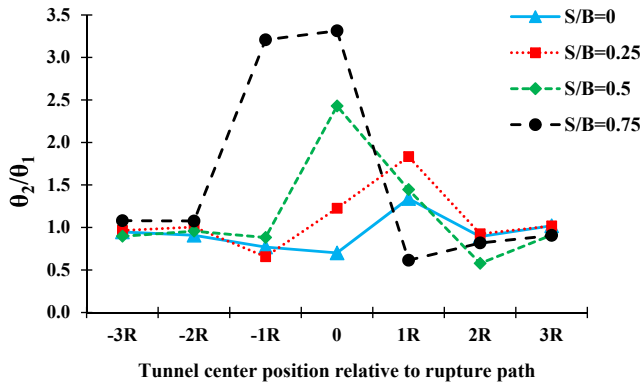


Fig. 11. The ratio of foundation rotations in two cases of with/without $[(\theta_2)/(\theta_1)]$ a tunnel with the diameter of $D = 4$ m. R is the tunnel radius.

in Table 1. The bending moment mounted on the principal directions of the tunnel cross section (North, East, South, West) and directions of the intermediate tunnel cross section (North East, South East, South West, North West) (see Fig. 1(b)).

The numerical analysis was conducted in two steps. Gravity loading was first applied to the model and then, to simulate fault movement, the right part of the model (hanging wall) moved at the dip angle of 60° , while the left part of the model remained immovable (the vertical throw of hanging wall was $h = 4$ m). The vertical boundaries were free to move in vertical direction and the horizontal boundaries were completely fixed.

An elasto-plastic constitutive model adopted by Mohr–Coulomb as a failure criterion with isotropic softening and presented by Anastopoulos and Gazetas (2007b) was employed to simulate the soil behavior. In this constitutive model, softening is introduced by reducing the mobilized friction angle φ_{mob} , while the mobilized dilation angle ψ_{mob} is defined with the increase of plastic octahedral shear strain:

$$\varphi_{mob} = \begin{cases} \varphi_p - \frac{\varphi_p - \varphi_{res}}{\gamma_f^p} \gamma_{oct}^p & \text{for } 0 \leq \gamma_{oct}^p \leq \gamma_f^p \\ \varphi_{res} & \text{for } \gamma_{oct}^p \leq \gamma_f^p \end{cases} \quad (1)$$

$$\psi_{mob} = \begin{cases} \psi_p \left(1 - \frac{\gamma_{oct}^p}{\gamma_f^p} \right) & \text{for } 0 \leq \gamma_{oct}^p \leq \gamma_f^p \\ \psi_{res} & \text{for } \gamma_{oct}^p \leq \gamma_f^p \end{cases} \quad (2)$$

where φ_p and φ_{res} are the friction angle at peak and its residual value; ψ_p and ψ_{res} are the dilation angle at peak and its residual value; γ_{oct}^p and γ_f^p are the octahedral plastic shear strain and its value at the end of softening.

The results of the direct shear test conducted by Baziar et al. (2016) were used in this study to select the material parameters of the

numerical modeling. The computed parameters for the soil were $\gamma_f^p = 0.244$, $\varphi_p = 35^\circ$, $\varphi_{res} = 30.2^\circ$ and $\psi_p = 6^\circ$. The foundation was modeled as a linear elastic element with high rigidity and 1 m thickness. In the contact surface between the foundation and soil, normal behavior of friction was considered with the friction coefficient of $0.7 \tan(\varphi)$. The tunnel was modeled using shell elements, and the behavior was assumed as linear elastic with typical properties of concrete. The interface between the tunnel and the surrounding soil was modeled as “hard” contact, while a normal behavior of friction with the friction coefficient of μ was used. Properties of the material used for the numerical simulation are presented in Table 2.

Due to the possibility of separation at the contact between the soil and tunnel or foundation, gap element was also introduced to the model. Gap elements are rigid in compression, but tensionless, allowing for the detachment at structure-soil interface.

The shear zone thickness was found to be dependent on the mesh size d_{FE} . However, with $d_{FE} \leq 1$ m, the orientation of the propagation path and the outcropping location would not be sensitive to the mesh density, provided that the scale similarity was maintained (Anastopoulos et al., 2009). The element chosen for soil, foundation and tunnel was quad-dominated with the width of 0.5 m or less. Meshing was denser near the tunnel. Fig. 2 shows finite element meshing used in the numerical modeling.

An explicit dynamic analysis can be used to perform quasi-static analyses (ABAQUS, 2014). The ABAQUS Dynamic/Explicit can produce results even when the mesh distortion is possible and the model might not converge for very large deformations (Baziar et al., 2016; Ni et al., 2018). Therefore, the explicit dynamic analysis was used to model the fault rupture propagation through the soil.

The effectiveness of a trench filled with EPS near the foundation on fault rupture-foundation-tunnel interaction was also investigated. An EPS wall with the depth of $H = 6$ m and width of $w = 1.5$ m was installed next to the foundation where a tunnel with the diameter of 4 m existed at the depth of 10 m (Fig. 3). Properties of the EPS used in the numerical modeling are described in Table 3.

3. Verification of the numerical model

The ability of numerical simulations in predicting the faulting effects on surface and underground structures was validated using centrifuge model tests conducted by Ashtiani et al. (2016) and Baziar et al. (2014b).

Ashtiani et al. (2016) conducted a series of 50-g centrifuge tests to investigate the effect of foundation embedment depth and contact pressure on the interaction of reverse faults and shallow foundations. All models were prepared using Firoozkuh sand No. 161 with a relative density of 60% ($D_r = 60\%$) and unit weight of 15.77 kN/m^3 . Direct shear tests were conducted, which led to $\varphi_p = 33^\circ$, $\varphi_{res} = 31^\circ$ and $\psi_p = 1^\circ$. Fig. 4 depicts the schematic configuration of the intended

Table 4
Vertical displacement of the foundation in numerical modeling.

	S/B	Without Tunnel	x = -3R	x = -2R	x = -R	x = 0	x = R	x = 2R	x = 3R
y = 8 m and D = 4 m	0	0.93 m	0.93 m	0.88 m	0.85 m	1.02 m	1.07 m	0.82 m	0.94 m
	0.25	0.46 m	0.52 m	0.45 m	0.43 m	0.74 m	0.47 m	0.41 m	0.48 m
	0.5	0.11 m	0.11 m	0.07 m	0.18 m	0.4 m	0.04 m	0.03 m	0.08 m
	0.75	0.08 m	0.07 m	0.08 m	0.05 m	0.03 m	0.11 m	0.08 m	0.08 m
y = 8 m and D = 6 m	0	0.93 m	0.96 m	0.92 m	0.77 m	1.08	1.1	0.87	0.94
	0.25	0.46 m	0.52	0.51	0.35	0.86	0.53	0.45	0.47
	0.5	0.11 m	0.13	0.13	0.14	0.64	0.05	0.05	0.09
	0.75	0.08 m	0.05	0.06	0.04	0.31	0.12	0.08	0.08
y = 10 m and D = 4 m	0	0.93 m	0.94	0.91	0.82	0.96	1.08	0.85	0.95
	0.25	0.46 m	0.48	0.5	0.37	0.72	0.51	0.44	0.47
	0.5	0.11 m	0.13	0.1	0.09	0.35	0.06	0.03	0.1
	0.75	0.08 m	0.08	0.08	0.03	0.01	0.12	0.09	0.08

Table 5
Horizontal displacement of the foundation in numerical modeling.

	S/B	Without Tunnel	x = -3R	x = -2R	x = -R	x = 0	x = R	x = 2R	x = 3R
y = 8 m and D = 4 m	0	2.01	1.96	1.99	1.73	1.99	2.53	1.89	2.01
	0.25	1.39	1.39	1.39	1.1	1.76	1.7	1.25	1.39
	0.5	0.69	0.66	0.62	0.71	1.29	0.77	0.49	0.63
	0.75	0.26	0.29	0.27	0.5	0.44	0.18	0.24	0.25
y = 8 m and D = 6 m	0	2.01	1.9	1.99	1.7	1.96	2.59	1.93	2.05
	0.25	1.39	1.32	1.42	1.03	1.78	1.68	1.35	1.42
	0.5	0.69	0.66	0.7	0.62	1.58	0.81	0.59	0.66
	0.75	0.26	0.3	0.31	0.47	1.08	0.16	0.26	0.25
y = 10 m and D = 4 m	0	2.01	2.04	1.97	1.84	1.87	2.47	1.89	2.04
	0.25	1.39	1.36	1.41	1.1	1.64	1.62	1.3	1.41
	0.5	0.69	0.7	0.67	0.58	1.13	0.81	0.55	0.65
	0.75	0.26	0.28	0.27	0.36	0.49	0.18	0.24	0.26

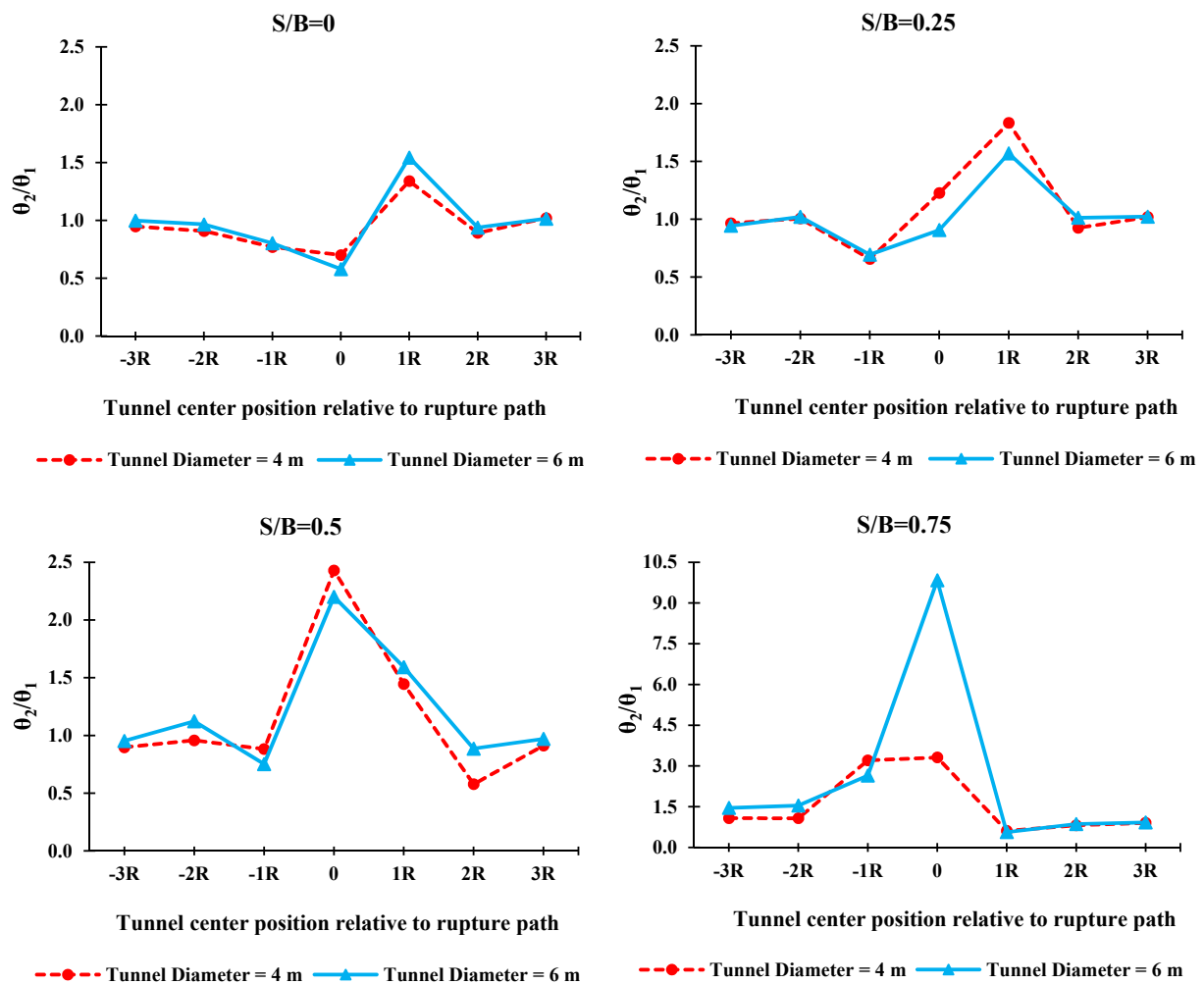


Fig. 12. The ratio of foundation rotation in the presence of a tunnel (θ_2) to foundation rotation without a tunnel present (θ_1) for different foundation positions (S/B). R is the tunnel radius. The tunnels are at the depth of y = 8 m.

study for verification of numerical model. The linear dimensions of the model (such as dimensions of the foundation, soil depth and displacements) are 1/50th of those of the prototype. The box was composed of a stationary footwall, a movable hanging wall, and a hydraulic jack. The movable hanging wall can be actuated by a hydraulic jack. Reverse fault displacement was applied to the sand layer with a dip angle of 60° (Fig. 4). The maximum vertical component of the fault displacement was 42.6 mm.

Baziar et al. (2014b) carried out several centrifuge tests under 80-g centrifugal acceleration to investigate the interaction of reverse fault

rupture propagation in the dry sand layer and existing tunnel. Quartz sand with a unit weight of 15–16 kN/m³ and a relative density of 50 and 70% was used for all the centrifuge model tests. The model-to-prototype scale was 1/80, and it was subjected to an acceleration of 80-g. The value of γ_f^p was 0.244 for $D_r = 70\%$, while $\varphi_p = 35^\circ$, $\varphi_{res} = 30.2^\circ$ and $\psi_p = 6^\circ$ (Baziar et al., 2016). The tunnel lining was modeled using aluminum alloy (6061-T6) frames. The upward movement increased while the vertical displacement of the surface was being recorded at increments of 2.5 mm of the fault throw, corresponding to

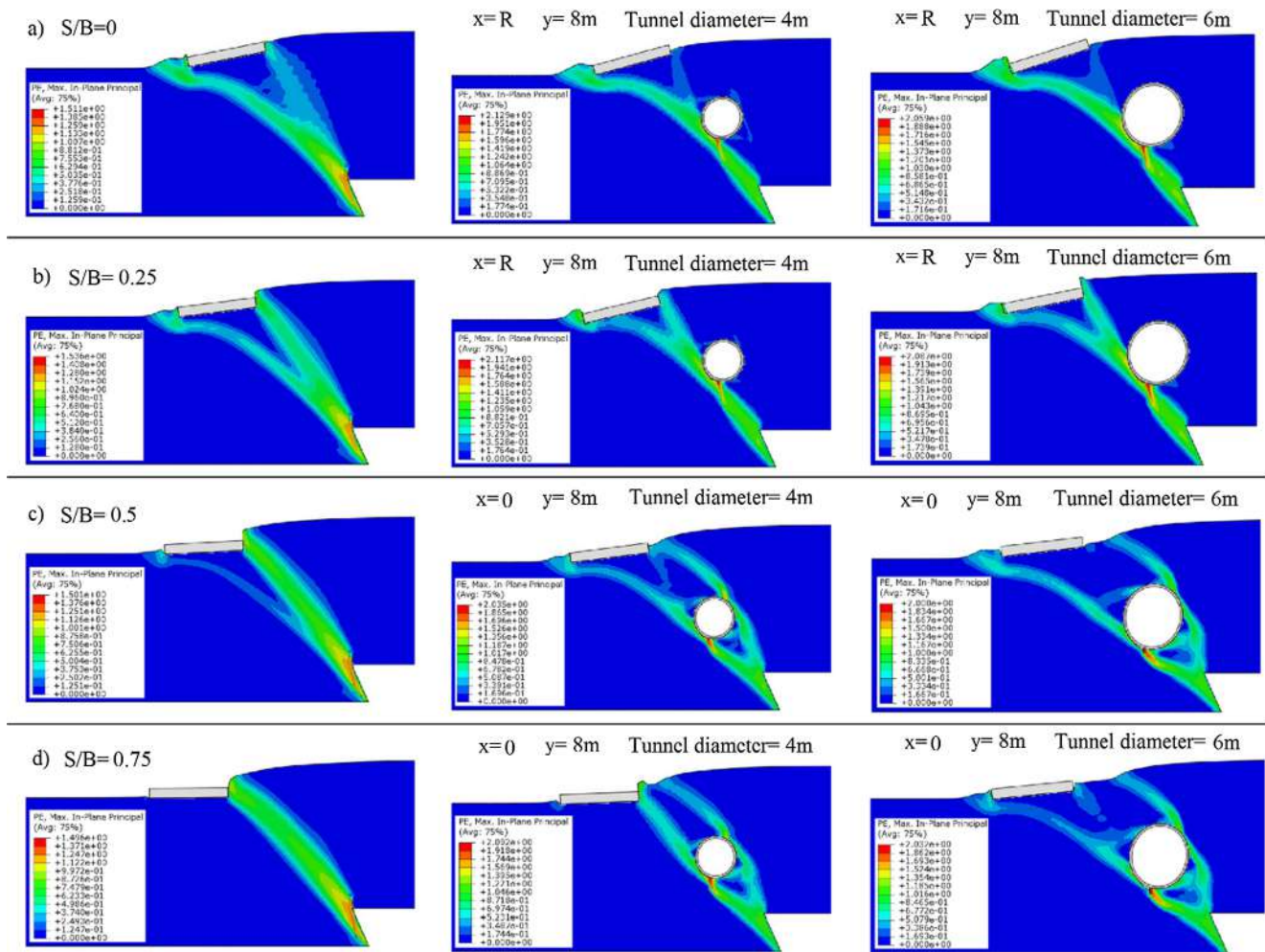


Fig. 13. The effect of the presence of a tunnel with different diameters, embedded at the depth of $y = 8\text{ m}$, on reverse fault (60°)–foundation interaction (FE computed plastic strain contours) at $h = 4\text{ m}$. x is the horizontal distances from the rupture path. R is the tunnel radius.

0.2 m of the prototype model. The maximum upward movement, with the 60° dip angle of faulting, was 50 mm (4 m in prototype). A tunnel with the diameter of $D = 4.24\text{ m}$ and thickness of $t = 0.24\text{ m}$ in prototype scale was placed in the position shown in Fig. 5.

3.1. Reverse fault–foundation interaction

Free-field fault rupture can be used to determine the fault rupture path as well as to select the different positions (S) of the foundation with respect to its emergence (Fig. 4). Fig. 6a and b compares the numerical modeling and experimental results at $h = 42.6\text{ mm}$ for free-field fault rupture, and the results were satisfactory. After determining the fault outcrop in free-field condition, the foundation was placed on the ground surface and at an $S/B = 0.75$ position. As shown in Fig. 6c and d, the shear zone predicted by the numerical analysis is similar to the centrifuge model. The foundation rotation versus the bedrock fault offset shown in Fig. 7 indicates good agreement between the numerical modeling and experimental results. The incremental rate of foundation rotation with increasing vertical displacement in numerical and experimental results is similar. The maximum difference between finite element analysis and experimental result is less than 0.2° .

3.2. Interaction between reverse faulting and tunnel

In free-field condition, the width of the failure region in the numerical analysis is nearly equal to that of the centrifuge model (Fig. 8a

and b). Fig. 9a shows the vertical displacement profiles at the ground surface for the 4 m throw of the hanging wall. As seen, the numerical model correlates well with the experimental results.

The effect of the presence of a tunnel on the fault rupture path and surface displacement for $h = 4\text{ m}$ was shown in Fig. 8c and d. The presence of a tunnel creates two separate rupture paths, and the two paths predicted by the numerical studies in the plastic strain zone are very similar with the results of the centrifuge model. Fig. 9b compares the experimental results and finite element analysis in terms of vertical displacement on the ground surface. The numerical modeling prediction for the location of the fault outcrop on the surface is almost accurate. However, the difference between the numerical and experimental results can be due to the assumption of the soil as a continuous media in the finite element analysis, while in reality it is a particular media. Soil surface disturbance is highly variable, and the FE continuum model may not fully reflect the soil disturbance behavior (Baziar et al., 2016).

4. Parametric study

4.1. Effect of the presence of tunnel on reverse fault–foundation interaction

Free-field fault rupture can help determine the fault rupture path corresponding to the fault angle 60° as well as selecting the different positions (S) of the foundation and tunnel location (x, y) (Fig. 1). In order to compare the foundation rotation for both with/without tunnel

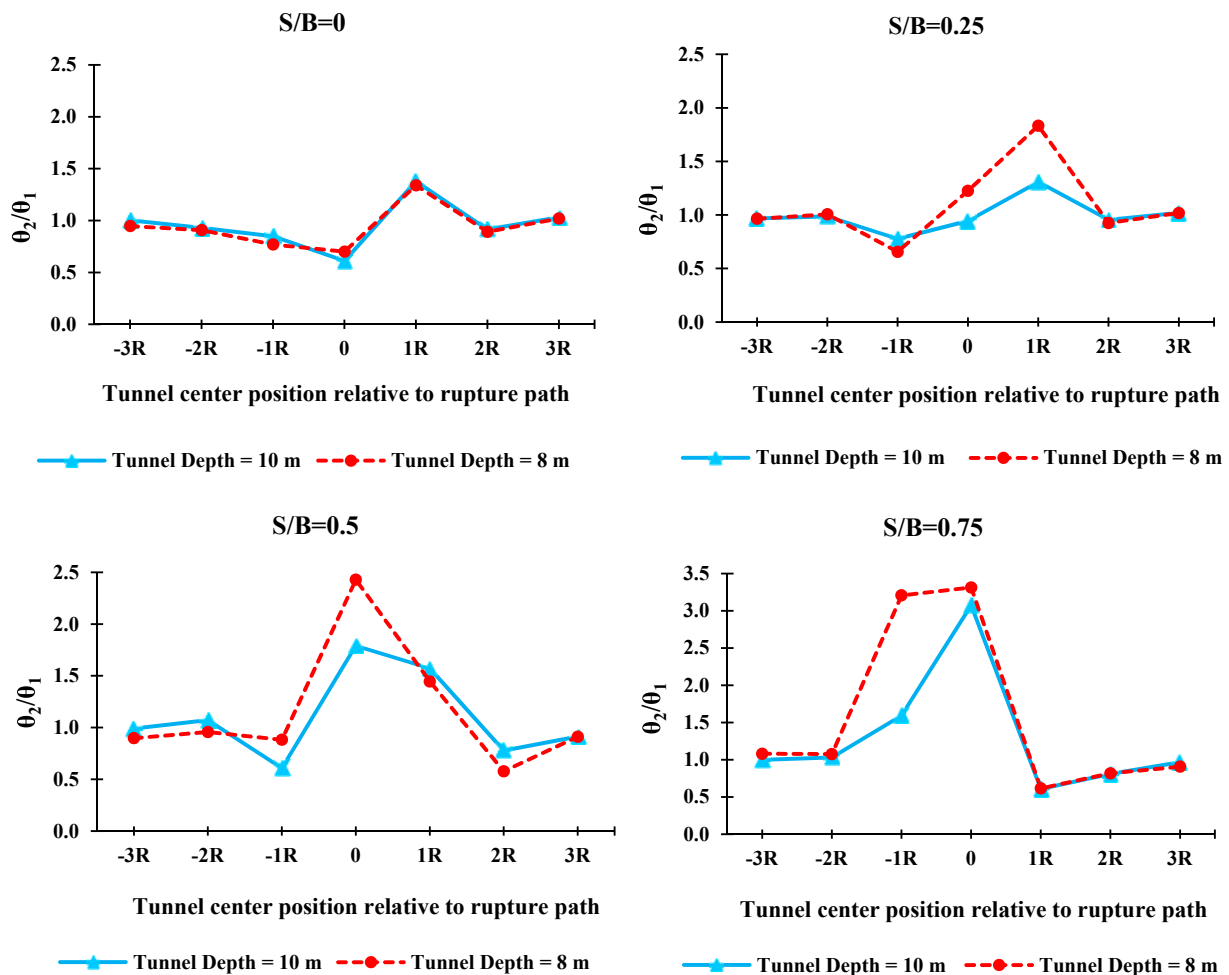


Fig. 14. Ratio of foundation rotation in the presence of the tunnel (θ_2) to foundation rotation without a tunnel present (θ_1) for different positions (S/B). R is the tunnel radius. The tunnels diameter is 4 m ($D = 4$ m).

presence conditions, the interaction between fault and shallow foundation without a tunnel was examined. The rotation of the foundation for $S/B = 0, 0.25, 0.5, 0.75$ and 1 were $11.0, 7.1, 3.0, 0.6$ and 0.2° , respectively. A tunnel with a diameter of $D = 4$ m and thickness of $t = 0.24$ m was embedded in the depth of $y = 8$ m in different horizontal distances from the rupture path (in free-field condition). Fig. 10 shows the results of the numerical analysis for the position of the tunnel, which has been the most rotation of foundation at $h = 4$ m. Fig. 11 illustrates the foundation rotation ratios with a tunnel (θ_2) to those without a tunnel (θ_1) for different positions (S/B) of the foundation. Since the foundation rotation in $S/B = 1$ is very small (less than one degree), it was neglected and not shown in the diagram. Fig. 11 shows that when the tunnel is situated in the rupture path, it can increase the foundation rotation. For example, the foundation rotation in $S/B = 0.75$ and 0.5 were 3.3 and 2.4 times more than the values of the case with no tunnel. The vertical and horizontal displacements of the foundation (the center of mass) is summarized in Tables 4 and 5, respectively. In some cases, the tunnel presence increased the vertical and horizontal displacement of the foundation. Following the placement of the tunnel with a diameter of $D = 4$ m in position ($x = 0$ and $y = 8$ m), the horizontal and vertical displacement of the foundation positioned at $S/B = 0.5$ increased by 0.6 m and 0.29 m after 4 m vertical throw of fault.

Fig. 10 illustrates the existence of a tunnel changes the fault rupture path. In some cases, ($S/B = 0, 0.25$ and 0.5), tunnel presence causes the plastic zone to distribute below the foundation and the left side of the foundation to move downward, thereby, increasing the foundation

rotation. For $S/B = 0.5, 0.75$ and 1 , the width of shear zone was wider in the soil profile and on the ground surface, compared to the cases without a tunnel. Furthermore, the presence of a tunnel created two separate rupture paths in such cases. Therefore, the right side of the foundation moved upward and the left side remained on the footwall, causing a differential displacement that was added to the foundation rotation.

4.2. The effect of tunnel diameter on reverse fault–foundation interaction

To investigate the effect of tunnel diameter on the fault rupture path and the foundation rotation, cases $D = 6$ m were compared with $D = 4$ m (under the same conditions); where D is the diameter of the tunnel. Fig. 12 shows similar trends among rotational ratios (θ_2/θ_1) that are in the presence of a tunnel with different diameters. The rotational ratios (θ_2/θ_1) in the foundation positioned at $S/B = 0.75$ for tunnel with diameter of $D = 6$ m is much higher than tunnel with diameter of $D = 4$ m because the plastic zone is distributed below the foundation and it can lead to an increase in the foundation rotation (see Fig. 13d). Fig. 13 displays the finite element deformed mesh with plastic strain contours for the case in which the tunnel caused the maximum rotation of the foundation. As shown in the figure, the general failure pattern and shear plane location near the tunnel did not significantly change by varying the tunnel diameter. However, the comparison of plastic strain contours having two separate rupture paths confirms the fact that a tunnel with a larger diameter cause the rupture path to deviate and propagate in a bigger area into the soil layer, causing the zone of

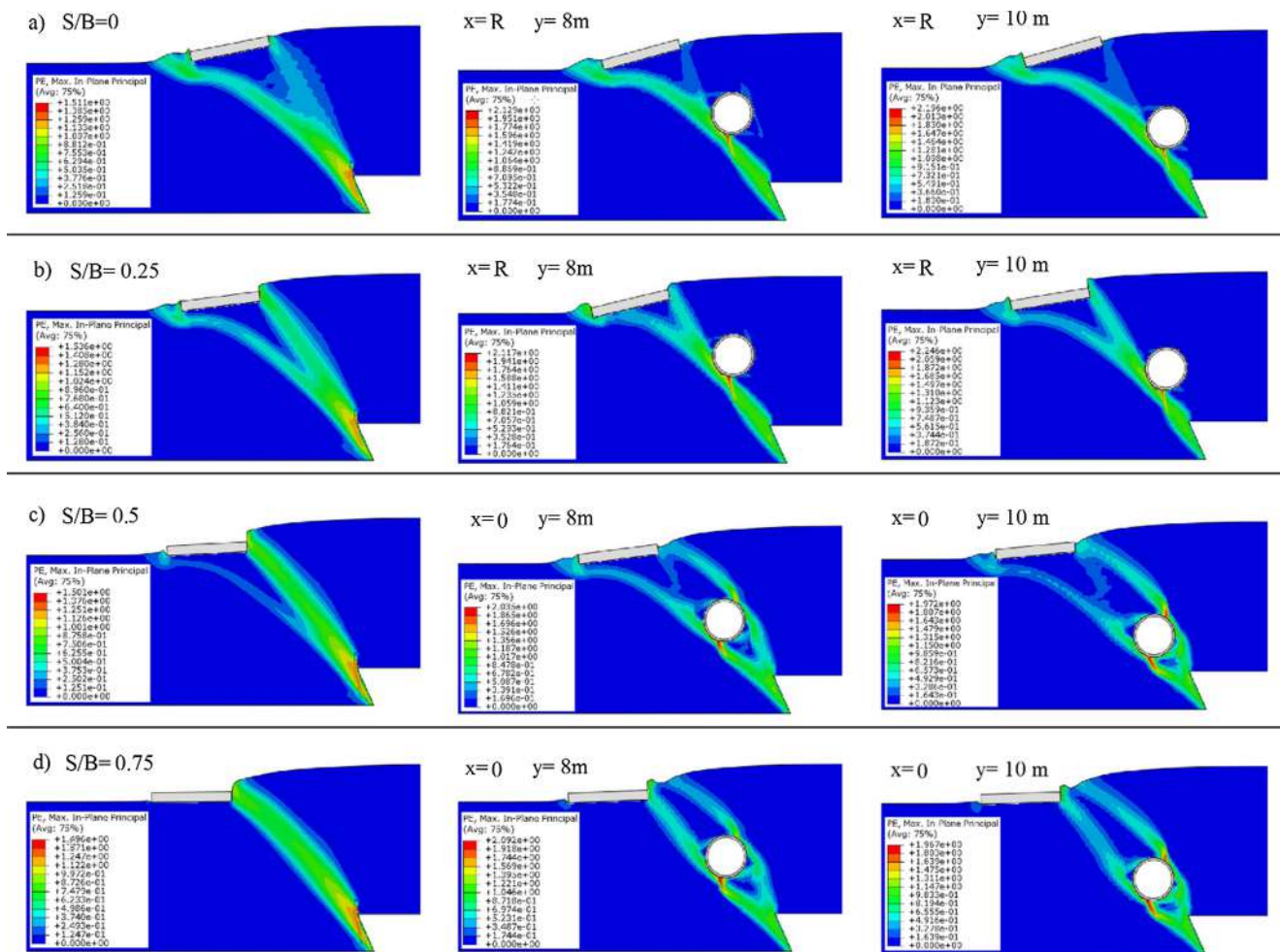


Fig. 15. Effect of the presence of tunnel with diameter of $D = 4\text{ m}$ in different depth (y) on reverse fault (60°)–foundation interaction (FE computed plastic strain contours) at $h = 4\text{ m}$. x is horizontal distances from the rupture path. R is the tunnel radius.

surface deformation to extend in a wider area (for example, see $S/B = 0.5$ and 0.75 in Fig. 13). Also for $S/B = 0.75$, the rupture path reached the left side of the foundation and the soil plastic zone changed. As a result, the left side surface subsidence decreased and the foundation rotation increased. As seen in Tables 4 and 5, the increase in the diameter of the tunnel can affect the horizontal and vertical displacement of the foundation. A tunnel ($x = 0$) with a diameter of 6 m increases the horizontal and vertical displacement of the foundation positioned at $S/B = 0.5$ by 22% and 60%, respectively, compared to a tunnel with a diameter of 4 m .

4.3. The effect of tunnel depth on reverse fault–foundation interaction

To investigate the effect of tunnel depth (y), the depth for a tunnel ($D = 4\text{ m}$) changed from 8 m to 10 m . Fig. 14 compares the foundation rotations for the intended tunnel at different depths. As seen, the trend of the rotational ratio (θ_2/θ_1) does not change by increasing the tunnel depth. However, Fig. 14 clearly shows that for $S/B = 0.25, 0.5$ and 0.75 , the rotation ratio for a deeper tunnel ($y = 10\text{ m}$) located in the shear zone is more than the one at a lower depth ($y = 8\text{ m}$). Increasing the tunnel depth inclines the left branch of the rupture path more towards the footwall, and the shear zone is extended over a wider area (Fig. 15). This causes the plastic zone to move away from the foundation at $S/B = 0.25$ and 0.5 and decreases the rotation. Results of the numerical modeling in Fig. 15c and d show that the concentration of maximum plastic strain contours is higher around the tunnel situated at a higher depth than the one at a lower depth. The results in Tables 4

and 5 indicate that the changes made in the horizontal and vertical displacements of the foundation for the tunnel at different depths are insignificant.

4.4. The mechanical response of tunnel lining

Figs. 16–18 illustrates diagrams of the bending moment and stress contours of the tunnel cross section shown in Figs. 10, 13 and 15, respectively. It can be seen that variation of the bending moment for the vertical throw of less than 1 m is significant. Therefore, vertical displacement of the fault up to 1 m has a clear impact on increasing the bending moments in the tunnel lining. Increasing the buried depth of the tunnel also increases the stresses and bending moments on the tunnel. For example, in $S/B = 0.5$ (Figs. 16 and 18), increasing the burial depth of the tunnel increases the maximum bending moment on the tunnel by about 33%. This increase can be due to the fact that increasing the depth increases the confining pressure as well. When the tunnel position is brought closer to the bedrock fault, the faulting pressure is propagated in the small area of the soil before reaching to the tunnel. Therefore, there is a higher faulting pressure on the tunnel. A comparison of the results between the $D = 4\text{ m}$ tunnel (Fig. 16) and the $D = 6\text{ m}$ tunnel (Fig. 17) indicates that increasing the diameter of the tunnel also increases the stress and bending moment.

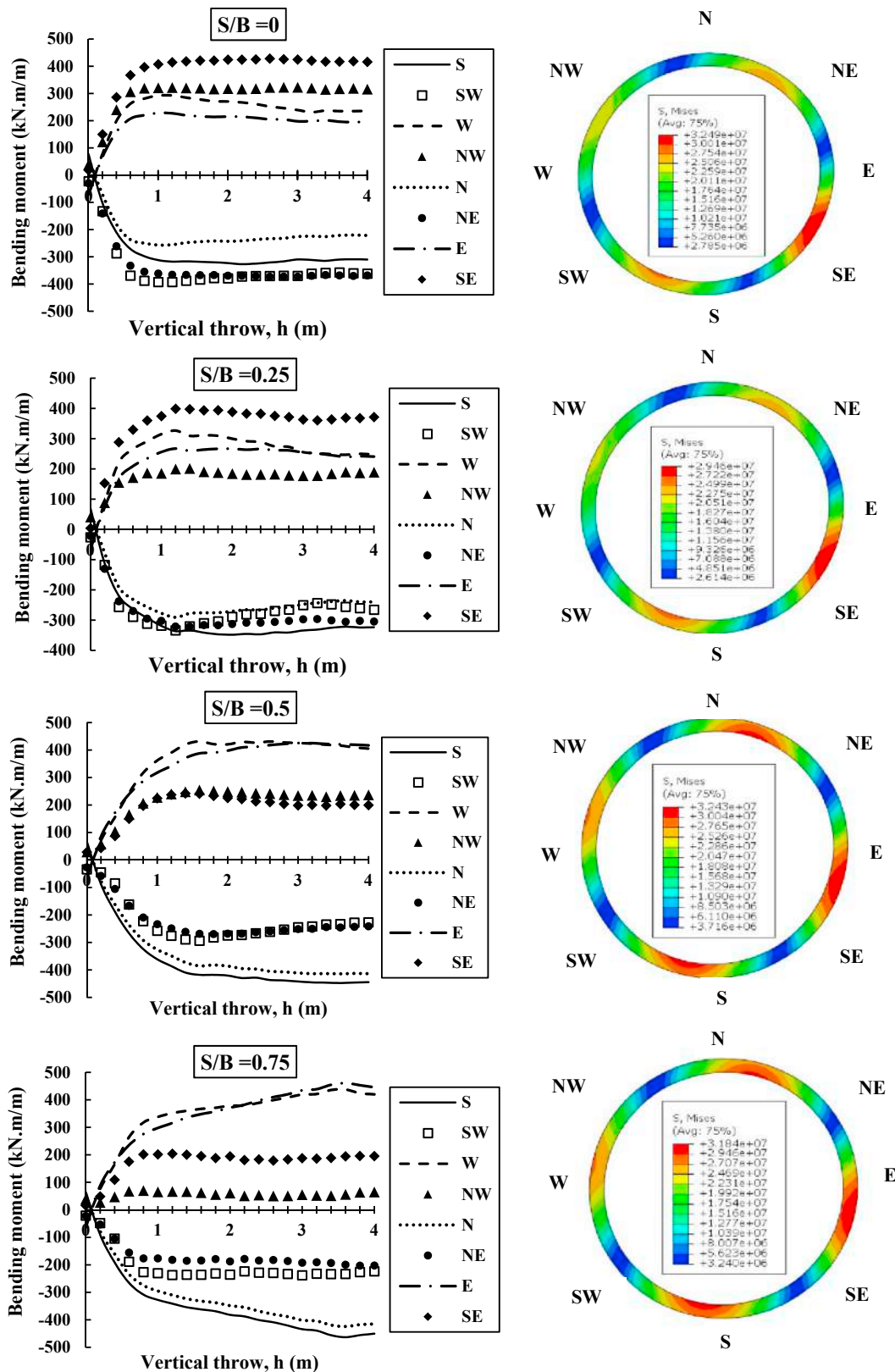


Fig. 16. Variation of bending moment in principal and intermediate directions of tunnel cross section in Fig. 10 against vertical throw of fault. Stress contours after 4 m vertical throw of fault are shown.

5. Mitigation of surface fault rupture hazard for shallow foundation by expanded polystyrene sheets (EPS)

In order to investigate the effect of a trench filled with EPS on the

fault rupture-foundation-tunnel interaction, an EPS wall with depth of $H = 6$ m and width of $w = 1.5$ m is installed next to the foundation in the presence of a tunnel with diameter of 4 m, located at the depth of 10 m (Fig. 3).

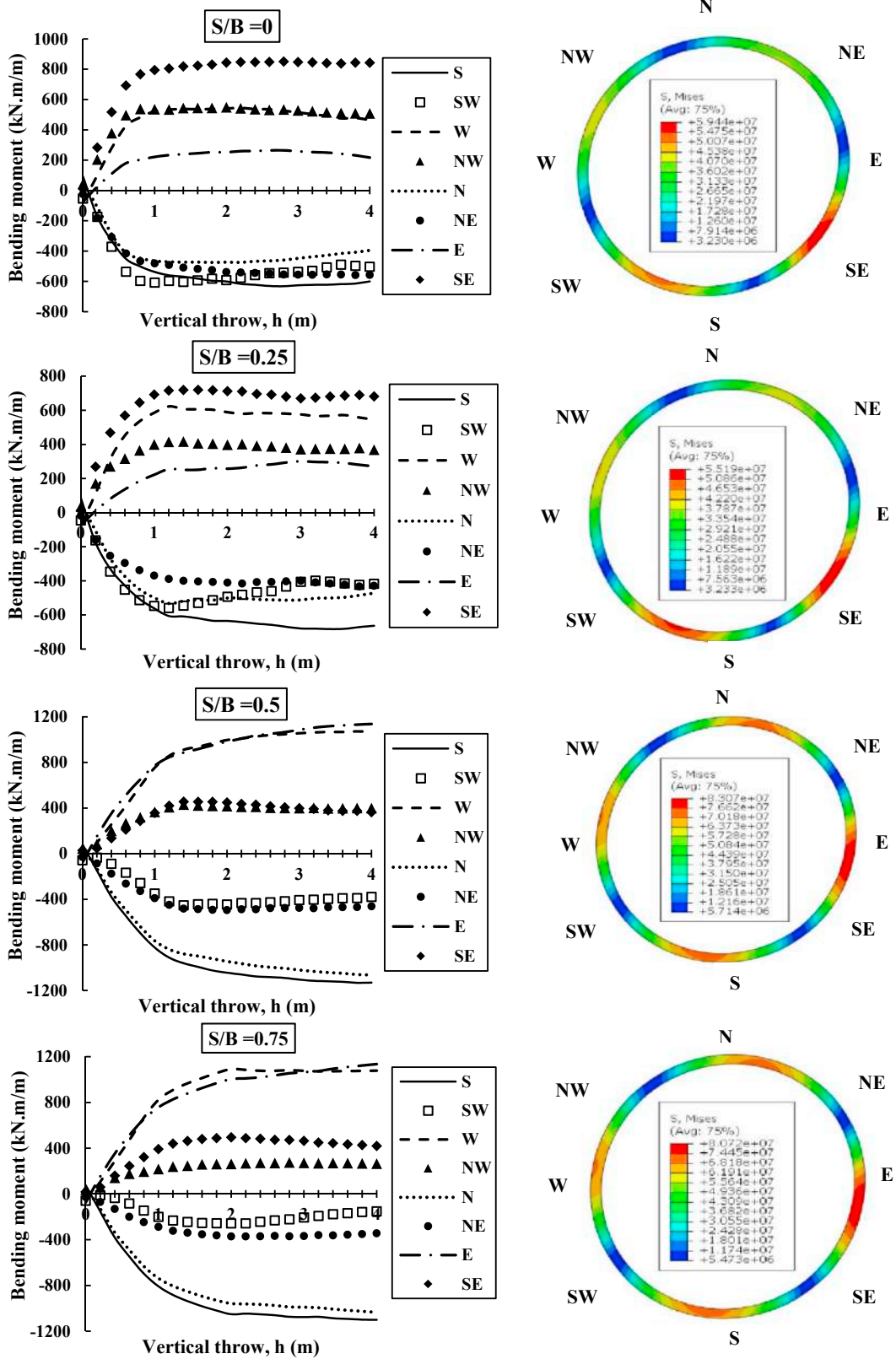


Fig. 17. Variation of bending moment in principal and intermediate directions of tunnel cross section in Fig. 13 against vertical throw of fault. Stress contours after 4m vertical throw of fault are shown.

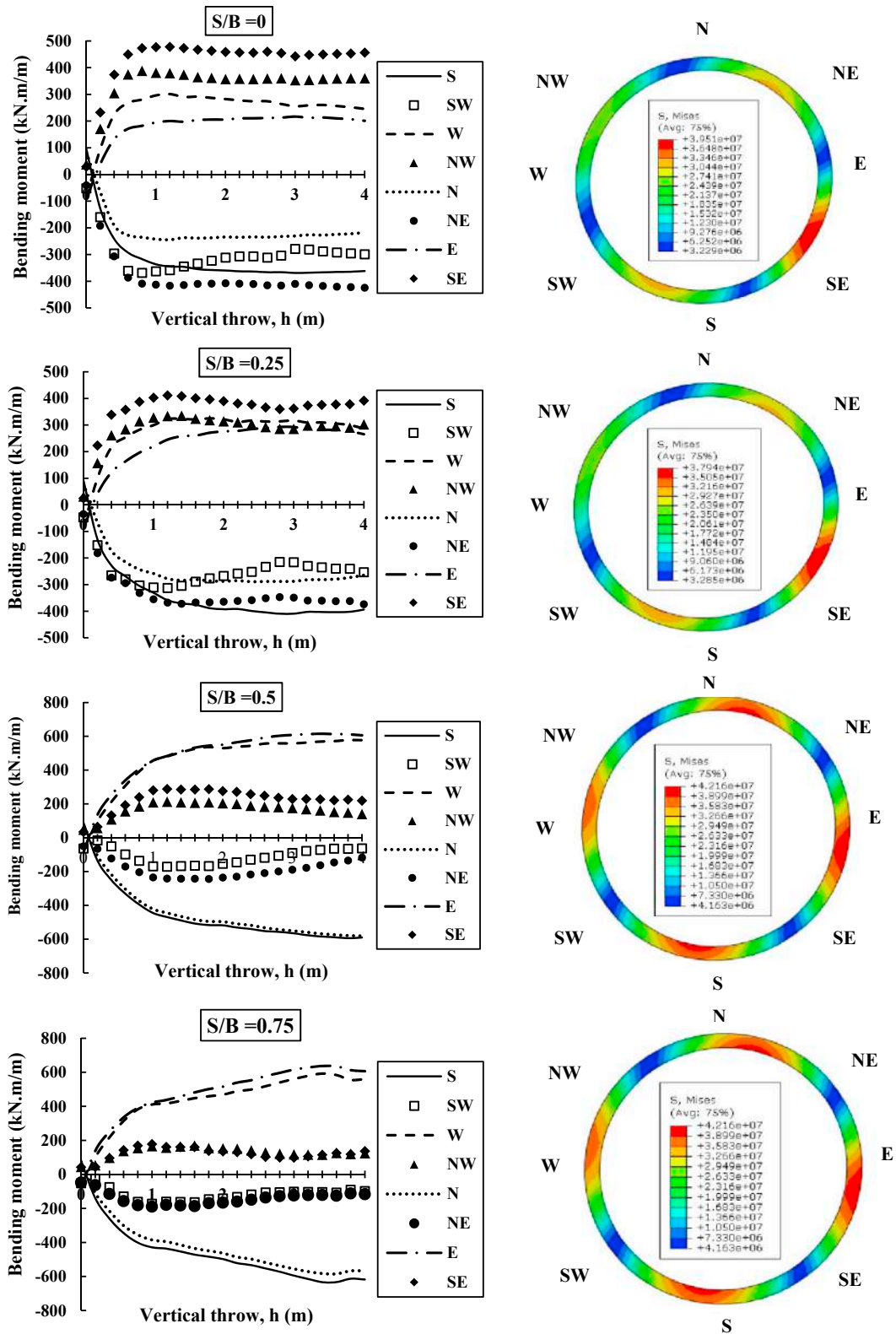


Fig. 18. Variation of bending moment in principal and intermediate directions of tunnel cross section in Fig. 15 against vertical throw of fault. Stress contours after 4 m vertical throw of fault are shown.

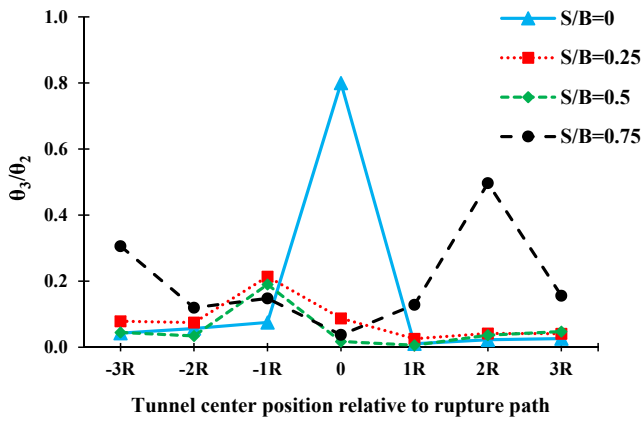


Fig. 19. Ratio of foundation rotation in the presence of the tunnel with diameter of $D = 4\text{ m}$ and EPS wall (θ_3) to foundation rotation without EPS wall (θ_2). R is the tunnel radius.

As seen in Fig. 19, the EPS wall installed next to the foundation could effectively reduce the rotation for all the foundation positions. This material possesses a low shear strength and high compressibility, which allows it to absorb fault induced rupture. The effectiveness of the EPS wall in mitigating the surface fault rupture and reducing the foundation rotation is shown in Fig. 20. The figure also depicts the plastic strain contours obtained by numerical analysis for maximum rotation (θ_3/θ_2). θ_3 is the ratio of foundation rotation in the presence of a tunnel and EPS wall, and θ_2 is the foundation rotation without an EPS wall. The mitigating effect for $S/B = 0$, when $x = 0$, is small (see Fig. 19) because the wall has not been able to fully absorb the fault rupture, and the left branch of the rupture has reached the other side of the foundation (see Fig. 20). This shows that the effectiveness of the EPS wall depends mainly on the geometry and location of the wall to intercept the fault rupture and deviate its path.

6. Conclusions

This study used a finite element methodology to analyze the impact of the tunnel on the interaction between the reverse fault and shallow foundation. This has allowed investigation of the effects of foundation

position (relative to the fault outcrop on the surface in free-field condition (S/B)), tunnel depth, horizontal tunnel distance relative to rupture path in free-field condition and tunnel diameter on the foundation response in fault zone. The numerical simulation was verified with the experimental results conducted by Ashtiani et al. (2016) and Baziar et al. (2014b). According to the results, the soil constitutive model that was used showed reliable predictions for the shear zone in the soil, the location of fault ruptures and the displacement profiles at the ground surface. The following conclusions can be made from this research:

- The existence of a tunnel in the shear zone changes the fault rupture path. In some cases, ($S/B = 0, 0.25$ and 0.5), the presence of the tunnel extends the plastic zone to under the foundation, leading to an increase in the rotation of the foundation. In the cases of $S/B = 0.5, 0.75$ and 1 , the tunnel causes the shear zone to be wider in the soil profile as well as the ground surface. The presence of a tunnel creates two separate rupture paths. This causes the right corner side of the foundation to move upward, while the left corner remains on the footwall. As a result, a differential displacement is obtained, which results in an increased rotation of the foundation.
- The general pattern of failure and the location of shear planes near the tunnel do not significantly change with variations of the tunnel diameter. However, the comparison of plastic strain contours for cases in which the tunnel causes the rupture path to be divided in two separate paths, demonstrates that a larger tunnel diameter causes the rupture to deviate and propagate in a wider area throughout the soil.
- Increasing the tunnel burial depth inclines a branch of the rupture path towards the footwall, and the shear zone is distributed on a wider area. This causes the plastic zone to move away from the foundation positioned at $S/B = 0.25$ and 0.5 and rotate less.
- The results showed that increasing the buried depth of the tunnel and its diameter increases the stresses and bending moments on the tunnel lining.
- As seen, existence of the tunnel in some cases increased the foundation rotation. The effectiveness of a trench filled with EPS near the foundation on fault rupture-foundation-tunnel interaction was investigated. EPS possesses a low shear strength and high compressibility, allowing it to absorb fault induced rupture and to mitigate the surface fault rupture, which in turn leads to less rotation of the foundation.

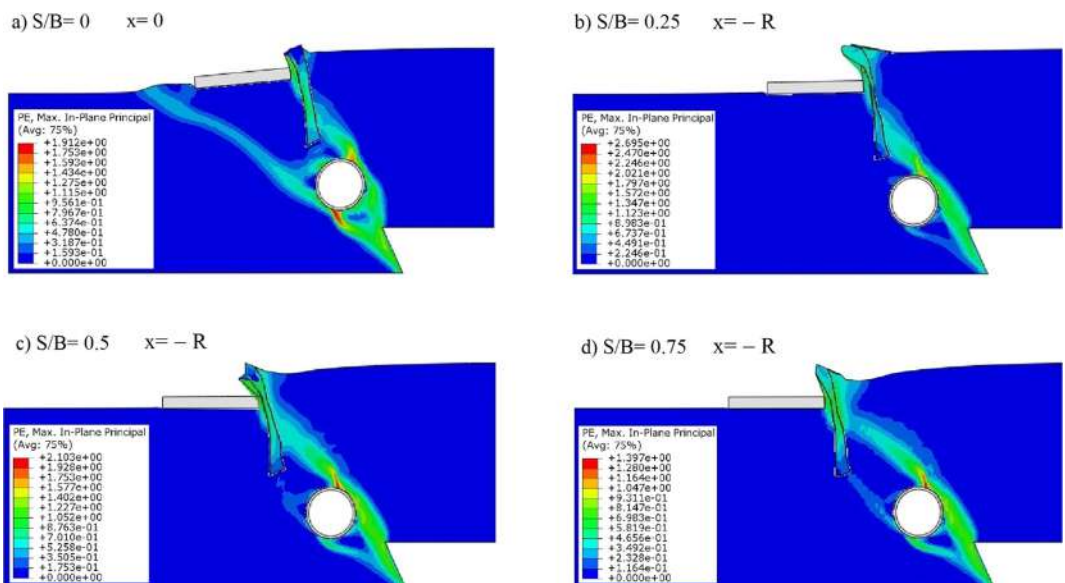


Fig. 20. Effect of EPS wall fault rupture-foundation-tunnel interaction at $h = 4\text{ m}$. The tunnel with diameter of $D = 4\text{ m}$ was embedded in depth of $y = 8\text{ m}$. x is horizontal distances from the rupture path. R is the tunnel radius.

Appendix A. Supplementary material

Supplementary data to this article can be found online at <https://doi.org/10.1016/j.tust.2019.04.005>.

References

- ABAQUS, 2014. ABAQUS V.6.14 user's manual, Providence, R.I.
- Ahmed, W., Bransby, M.F., 2009. The interaction of shallow foundations with reverse faults. *J. Geotech. Geoenviron. Eng.* 135 (7), 914–924.
- Anastasopoulos, I., Gazetas, G., 2007a. Foundation–structure systems over a rupturing normal fault: Part I. Observations after the Kocaeli 1999 earthquake. *Bull. Earthq. Eng.* 5 (3), 253–275.
- Anastasopoulos, I., Gazetas, G., 2007b. Foundation-structure systems over a rupturing normal fault: Part II. Analysis of the Kocaeli case histories. *Bull. Earthq. Eng.* 5 (3), 277–301.
- Anastasopoulos, I., Callerio, A., Bransby, M.F., Davies, M.C.R., El Nahas, A., Faccioli, E., Gazetas, G., Masella, A., Paolucci, R., Pecker, A., Rossignol, E., 2008a. Numerical analyses of fault–foundation interaction. *Bull. Earthq. Eng.* 6 (4), 645–675.
- Anastasopoulos, I., Gerolymos, N., Gazetas, G., Bransby, M.F., 2008b. Simplified approach for design of raft foundations against fault rupture. Part I: free-field. *Earthq. Eng. Eng. Vib.* 7, 147–163.
- Anastasopoulos, I., Gerolymos, N., Gazetas, G., Bransby, M.F., 2008c. Simplified approach for design of raft foundations against fault rupture. Part II: soil–structure interaction. *Earthq. Eng. Eng. Vib.* 7, 165–179.
- Anastasopoulos, I., Gazetas, G., Bransby, M.F., Davies, M.C.R., El Nahas, A., 2009. Normal fault rupture interaction with strip foundations. *J. Geotech. Geoenviron. Eng.* 135 (3), 359–370.
- Anastasopoulos, I., Gazetas, G., 2010. Analysis of cut-and-cover tunnels against large tectonic deformation. *Bull. Earthq. Eng.* 8 (2), 283–307.
- Ashtiani, M., Ghalandarzadeh, A., Towhata, I., 2016. Centrifuge modeling of shallow embedded foundations subjected to reverse fault rupture. *Can. Geotech. J.* 53 (3), 505–519.
- Ashtiani, M., Ghalandarzadeh, A., Mahdavi, M., Hedayati, M., 2018. Centrifuge modeling of geotechnical mitigation measures for shallow foundations subjected to reverse faulting. *Can. Geotech. J.* 55 (8), 1130–1143.
- Baziar, M.H., Nabizadeh, A., Jabbari, M., 2014a. Numerical modeling of interaction between dip-slip fault and shallow foundation. *Bull. Earthq. Eng.* 13 (6), 1613–1632.
- Baziar, M.H., Nabizadeh, A., Lee, C., Hung, W., 2014b. Centrifuge modeling of interaction between reverse faulting and tunnel. *Soil Dyn. Earthq. Eng.* 65, 151–164.
- Baziar, M.H., Nabizadeh, A., Mehrabi, R., Lee, C.J., Hung, W.Y., 2016. Evaluation of underground tunnel response to reverse fault rupture using numerical approach. *Soil Dyn. Earthq. Eng.* 83, 1–17.
- Berrill, J.B., 1983. Two-dimensional analysis of the effect of fault rupture on buildings with shallow foundations. *Int. J. Soil Dyn. Earthq. Eng.* 2 (3), 156–160.
- Bransby, M.F., Davies, M.C.R., El Nahas, A., 2008a. Centrifuge modeling of normal fault–foundation interaction. *Bull. Earthq. Eng.* 6 (4), 585–605.
- Bransby, M.F., Davies, M.C.R., El Nahas, A., Nagaoka, S., 2008b. Centrifuge modeling of reverse fault–foundation interaction. *Bull. Earthq. Eng.* 6 (4), 607–628.
- Bray, J.D., 2001. Developing mitigation measures for the hazards associated with earthquake surface fault rupture. In: *Workshop on Seismic Fault-induced Failures*. Japan Society for the Promotion of Science, University of Tokyo, pp. 55–80.
- Brennan, A., Roby, M., Bransby, F., Nagaoka, S., 2007. Fault rupture modification by blocky inclusions. 4th International Conference on Earthquake Geotechnical Engineering. Paper No 1480.
- El Nahas, A., Bransby, M.F., Davies, M.C.R., 2006. Interaction between normal fault rupture and rigid, strong raft foundations. In: *Proceedings of the Sixth International Conference on Physical Modeling in Geotechnics*, pp. 337–342.
- Faccioli, E., Anastasopoulos, I., Gazetas, G., Callerio, A., Paolucci, R., 2008. Fault rupture–foundation interaction: selected case histories. *Bull. Earthq. Eng.* 6 (4), 557–583. Special Issue: Integrated approach to fault rupture and soil–foundation interaction.
- Fadaee, M., Anastasopoulos, I., Gazetas, G., Jafari, M.K., Kamalian, M., 2013. Soil bentonite wall protects foundation from thrust faulting: analyses and experiment. *Earthq. Eng. Eng. Vib.* 12, 473–486.
- Gazetas, G., Anastasopoulos, I., Apostolou, M., 2007. Shallow and deep foundations under fault rupture or strong seismic shaking. *Earthq. Geotech. Eng. Geotech. Earthq. Eng.* 6, 185–215.
- Gazetas, G., Pecker, A., Faccioli, E., Paolucci, R., Anastasopoulos, I., 2008. Preliminary design recommendations for fault–foundation interaction. *Bull. Earthq. Eng.* 6 (4), 677–687.
- Karamanos, S.A., Sarvanis, G.C., Keil, B.D., Card, R.J., 2017. Analysis and design of buried steel water pipelines in seismic areas. *J. Pipeline Syst. Eng. Pract.* 8 (4) Article Number: 04017018.
- Kelson, K.I., Kang, K.H., Page, W.D., Lee, C.T., Cluff, L.S., 2001. Representative styles of deformation along the Chelungpu fault from the 1999 Chi-Chi (Taiwan) earthquake: geomorphic characteristic and responses of man-made structures. *Bull. Seismol. Am.* 91 (5), 930–952.
- Kiani, M., Akhlaghi, T., Ghalandarzadeh, A., 2016. Experimental modeling of segmental shallow tunnels in alluvial affected by normal faults. *Tunn. Undergr. Space Technol.* 51, 108–119.
- Konagai, K., 2005. Data archives of seismic fault-induced damage. *J. Soil Dyn. Earthq. Eng.* 25, 559–570.
- Konagai, K., Johansson, J., Zafeirakos, A., Numada, M., Sadr, A.A., 2005. Damage to tunnels in the October 23, 2004 Chuetsu earthquake. *J. Earthq. Eng.* 28, 1–8.
- Lazarte, C.A., 1996. The Response of Earth Structures to Surface Fault Rupture. Ph.D. Thesis. Department of Civil Engineering, University of California, Berkeley.
- Lettis, W., Bachhuber, J., Witter, R., 2000. Surface fault rupture. *Earthq. Spectra* 16 (S1), 11–53.
- Lew, M., Naeim, F., Huang, S.C., Lam, H.K., Carpenter, L.D., 2000. Geotechnical and geological effects of the 21 September 1999 Chi-Chi earthquake. *Taiwan. Struct. Des. Tall Build.* 9, 89–106.
- Lin, M.L., Chung, C.F., Jeng, F.S., Yao, T.C., 2007. The deformation of overburden soil induced by thrust faulting and its impact on underground tunnels. *Eng. Geol.* 92, 110–132.
- Loli, M., Anastasopoulos, I., Bransby, M.F., Ahmed, W., Gazetas, G., 2012. Interaction of caisson foundations with a seismically rupturing normal fault: centrifuge testing versus numerical simulation. *Geotechnique* 62 (1), 29–43.
- Moosavi, S.M., Jafari, M.K., Kamalian, M., Shafiee, A., 2010. Experimental investigation of reverse fault rupture–rigid shallow foundation interaction. *Int. J. Civ. Eng.* 8 (2), 85–98.
- Moosavi, S.M., Jafari, M.K., 2012. Investigation of the surface fault rupture hazard mitigation by geosynthetics. 15th World Conference on Earthquake Engineering.
- Ni, P., Moore, I.D., Take, W.A., 2018. Numerical modeling of normal fault–pipeline interaction and comparison with centrifuge tests. *Soil Dyn. Earthq. Eng.* 105, 127–138.
- Oettle, N.K., 2013. Earthquake Surface Fault Rupture Interaction with Building Foundations. Ph.D. Thesis. University of California, Berkeley.
- Oettle, N.K., Bray, J.D., 2013a. Fault rupture propagation through previously ruptured soil. *J. Geotech. Geoenviron. Eng.* 139 (10), 1637–1647.
- Oettle, N.K., Bray, J.D., 2013b. Geotechnical mitigation strategies for earthquake surface fault rupture. *J. Geotech. Geoenviron. Eng.* 139, 1864–1874.
- Pamuk, A., Kalkan, E., Linga, H.I., 2005. Structural and geotechnical impacts of surface rupture on highway structures during recent earthquakes in Turkey. *Soil Dyn. Earthq. Eng.* 25, 581–589.
- Prentice, C., Ponti, D., 1997. Coseismic deformation of the Wrights tunnel during the 1906 San Francisco earthquake: a key to understanding 1906 fault slip and 1989 surface ruptures in the southern Santa Cruz Mountains, California. *J. Geophys. Res.* 102 (B1), 635–648.
- Sarayloo, M., Mahinroosta, R., 2016. Analysis of the impacts of a tunnel on a normal fault rupture through uniform soil cover. Fourth Geo-China International Conference, Shandong, China.
- Schiff, A.J., Tang, A.K., 2000. Chi Chi, Taiwan Earthquake of September 21, 1999 Lifeline Performance. Technical Council on Lifeline Earthquake Engineering (TCLLEE), Monograph No.18, ASCE.
- Sugimura, Y., Miura, S., Konagai, K., 2001. Damage to Shihkang dam inflicted by faulting in the September 1999 Chichi earthquake. In: *Workshop on Seismic Fault-induced Failures*. Japan Society for the Promotion of Science, University of Tokyo, pp. 143–154.
- Tsai, K.C., Hsiao, C.P., Bruneau, M., 2000. Overview of building damages in 921 Chi-Chi earthquake. *Earthq. Eng. Eng. Seismol.* 2 (1), 93–108.
- Ulusay, R., Aydan, O., Hamada, M., 2002. The behaviour of structures built on active fault zones: examples from the recent earthquakes of Turkey. *Struct. Eng. Earthq. Eng.* 19 (2), 149–167.
- Wang, Z.Z., Zhang, Z., Gao, B., 2012. The seismic behavior of the tunnel across active fault. *Proceedings of the 15th World Conference on Earthquake Engineering*. Lisbon, Portugal.
- Wang, W.L., Wang, T.T., Su, J.J., Lin, C.H., Seng, C.R., Huang, T.H., 2001. Assessment of damages in mountain tunnels due to the Taiwan Chi-Chi Earthquake. *Tunn. Undergr. Space Technol.* 16, 133–150.
- Yilmaz, M.T., Paolucci, R., 2007. Earthquake fault rupture–shallow foundation interaction in undrained soils: a simplified analytical approach. *Earthq. Eng. Struct. Dyn.* 36 (1), 101–118.